THE JOURNAL OF BIOLOGICAL CHEMISTRY VOL. 287, NO. 43, pp. 36305–36311, October 19, 2012

Role of Detergents in Conformational Exchange of a G Protein-coupled Receptor*

Received for publication, July 31, 2012, and in revised form, August 9, 2012 Published, JBC Papers in Press, August 14, 2012, DOI 10.1074/jbc.M112.406371

Ka Young Chung[‡§1], **Tae Hun Kim**[¶1], **Aashish Manglik**[‡], **Rohan Alvares**[¶], **Brian K. Kobilka**[‡], **and R. Scott Prosser**[¶2]

From the [‡]*Department of Molecular and Cellular Physiology, Stanford University School of Medicine, Stanford, California 94305, the* [§]*School of Pharmacy, Sungkyunkwan University, Suwon 440-746, South Korea, and the* [¶]*Department of Chemistry, University of Toronto, Mississauga, Ontario L5L 1C6, Canada*

Background: Membrane protein functional dynamics are sensitive to the detergent host.
Results: Three functional states of the β_2-adrenoreceptor (β_2AR) are identified in maltose-neopentyl glycol, whereas all states exchange rapidly in dodecyl maltoside.
Conclusion: β_2AR converts between inactive and active states on a time scale that depends on the detergent off-rate.
Significance: G protein-coupled receptor functional dynamics are understood by considering topology changes and corresponding rearrangements of associated detergents.

The G protein-coupled β_2-adrenoreceptor (β_2AR) signals through the heterotrimeric G proteins G_s and G_i and β-arrestin. As such, the energy landscape of β_2AR-excited state conformers is expected to be complex. Upon tagging Cys-265 of β_2AR with a trifluoromethyl probe, ^{19}F NMR was used to assess conformations and possible equilibria between states. Here, we report key differences in β_2AR conformational dynamics associated with the detergents used to stabilize the receptor. In dodecyl maltoside (DDM) micelles, the spectra are well represented by a single Lorentzian line that shifts progressively downfield with activation by appropriate ligand. The results are consistent with interconversion between two or more states on a time scale faster than the greatest difference in ligand-dependent chemical shift (*i.e.* >100 Hz). Given that high detergent off-rates of DDM monomers may facilitate conformational exchange between functional states of β_2AR, we utilized the recently developed maltose-neopentyl glycol (MNG-3) diacyl detergent. In MNG-3 micelles, spectra indicated at least three distinct states, the relative populations of which depended on ligand, whereas no ligand-dependent shifts were observed, consistent with the slow exchange limit. Thus, detergent has a profound effect on the equilibrium kinetics between functional states. MNG-3, which has a critical micelle concentration in the nanomolar regime, exhibits an off-rate that is 4 orders of magnitude lower than that of DDM. High detergent off-rates are more likely to facilitate conformational exchange between distinct functional states associated with the G protein-coupled receptor.

Integral membrane proteins, which constitute one-third of the proteome, serve many physiological roles as receptors, transporters, channels, enzymes, and signal transducers. Among these membrane proteins, G protein-coupled receptors (GPCRs)[3] represent one of the most functionally and medically important classes of integral membrane proteins, given their key role in signal transduction and their propensity to respond to pharmacological agents. There are at least 350 non-odorant GPCRs, all of which are characterized by seven-transmembrane α-helical segments separated by intra- and extracellular loops (1). Although GPCRs share conserved sequence motifs and three-dimensional architecture, individual GPCRs may respond to a diverse range of stimuli, including light, hormones, and neurotransmitters. Moreover, GPCR pharmacology is complex, and most GPCRs exhibit varying degrees of activity in response to different ligands. As is the case for many ligand-activated GPCRs, the β_2-adrenoreceptor (β_2AR) couples the binding of specific agonists with the activation of either the stimulatory or inhibitory heterotrimeric G proteins G_s and G_i while alternatively signaling through MAPK pathways in a G protein-independent manner via β-arrestin (2). GPCR functional complexity may therefore arise from an ensemble of conformers corresponding to states that preferentially interact with specific signaling partners. It is key to identify states characterizing this ensemble and to distinguish their ligand-dependent equilibria and interconversion rates if we are to understand GPCR functional mechanisms.

X-ray crystallography has revealed detailed high resolution structures of both inactive and active states of GPCRs, providing a basis for explaining their pharmacology and mechanism of action (3). Solution-state NMR-based structures of GPCRs have been so far less forthcoming. However, in cases in which large integral membrane proteins of comparable complexity could be heterologously expressed and reconstituted in detergent micelles, high resolution structures have been determined by NMR (4–12). Notably, NMR studies of the microbial seven-helix 241-residue receptor phototaxis receptor sensory rhodopsin II suggested that GPCRs may be within reach of solu-

* This work was supported, in whole or in part, by National Institutes of Health Grant NH028471 (to B. K. K.). This work was also supported by Research Discovery Award 261980 from the Natural Sciences and Engineering Research Council of Canada (NSERC; to R. S. P.).
[1] Both authors contributed equally to this work.
[2] To whom correspondence should be addressed: Dept. of Chemistry, University of Toronto, UTM, 3359 Mississauga Rd. N., Mississauga, ON L5L 1C6, Canada. Tel.: 905-828-3802; E-mail: scott.prosser@utoronto.ca.

[3] The abbreviations used are: GPCR, G protein-coupled receptor; β_2AR, β_2-adrenoreceptor; CMC, critical micelle concentration; DDM, dodecyl maltoside; MNG, maltose-neopentyl glycol.

tion-state NMR (13). Many have noted that mutagenesis and detergent screening are key to identifying conditions for minimizing exchange broadening in polytopic α-helical membrane proteins (1, 13–16). However, it may be that NMR of GPCRs is further complicated by the complex landscape of receptor conformers, the populations and exchange rates of which conspire to give significant exchange broadening. In this work on human β_2AR, we demonstrate, by ^{19}F NMR, that detergents profoundly influence the rate of exchange between functional states and, consequently, spectral resolution. Moreover, we draw a connection between detergent off-rates, which differ by a factor of 10,000 in this study, and the rate of exchange between functional states in the GPCR. Conventional detergents with a critical micelle concentration (CMC) that falls in the 0.1 mM regime give rise to GPCR spectra that undergo fast or intermediate exchange between inactive and active states. A new class of detergent with a CMC in the nanomolar range gives rise to GPCR spectra that undergo slow exchange between three distinct states (17).

EXPERIMENTAL PROCEDURES

Δ4-β_2AR Generation, Purification, and Labeling with Bromotrifluoroacetone—Site-directed mutagenesis of β_2AR was performed using human β_2AR cDNA containing the FLAG epitope at the N terminus. As described previously (18), we utilized a minimal cysteine version of β_2AR with mutations C77V, C275S, C378A, and C406A.

Δ4-β_2AR was expressed in Sf9 insect cell (*Spodoptera frugiperda*) cultures (grown in ESF 921 medium, Expression Systems) infected with recombinant baculovirus (pFastBac, Expression Systems) and solubilized in *n*-dodecyl β-D-maltoside according to methods described previously (21). Insect cell cultures were grown in the presence of 1 μM alprenolol to increase protein yield.

Cell pellets were lysed by osmotic shock, the membrane fraction was isolated by centrifugation, and membranes containing Δ4-β_2AR were solubilized in buffer composed of 20 mM HEPES (pH 7.5), 100 mM NaCl, 1% dodecyl maltoside (DDM), 0.01% cholesterol hemisuccinate, and 1 μM alprenolol. M1 FLAG affinity chromatography (Sigma) served as the initial purification step, followed by alprenolol-Sepharose chromatography for selection of functional receptors. A subsequent M1 FLAG affinity chromatography step was used to wash out alprenolol and to exchange DDM into maltose-neopentyl glycol (MNG-3). The DDM sample was prepared as described previously (19). Δ4-β_2AR was loaded onto an M1 FLAG resin and washed with buffer (20 mM HEPES (pH 7.5), 100 mM NaCl, and 2 mM $CaCl_2$) containing 0.2% MNG-3 and eluted in buffer (20 mM HEPES (pH 7.5), 100 mM NaCl, 5 mM EDTA, and 200 μg/ml FLAG peptide) containing 0.01% MNG-3.

Detergent-exchanged Δ4-β_2AR was eluted and labeled with 3-bromo-1,1,1-trifluoroacetone at 4 °C overnight. 50 μM tris(2-carboxyethyl)phosphine was first added to reduce any cross-linked receptor, followed by 100 μM 3-bromo-1,1,1-trifluoroacetone. Free 3-bromo-1,1,1-trifluoroacetone was removed by desalting using a Zeba spin desalting column (Thermo Scientific) and concentrated with a 10-kDa molecular mass cutoff Vivaspin concentrator.

Isothermal Titration Calorimetry—The heats of DDM demicellization were obtained using a VP-ITC microcalorimeter (MicroCal Inc., Northampton, MA) at 30 °C. The sample cell was filled with buffer (20 mM HEPES (pH 7.5) and 100 mM NaCl) and had a volume of 1.455 ml. Injections (ranging from 2 to 10 μl) of dodecylphosphocholine micellar solution (3.68 mM) were added to the sample cell in 5-min intervals. The data were processed using MicroCal Origin software. ΔH_{mic} and CMC were extracted from the data as described elsewhere (20).

Surface Tension Experiments—Surface tension measurements were performed to determine the CMC of the MNG-3 samples. The surface tension was measured using a Sigma 70 tensiometer (KSV Instruments Ltd.) with a platinum Wilhelmy plate. Samples of increasing concentrations (5–50%) were prepared by diluting the stock solution (100 nM MNG-3) using 20 mM HEPES (pH 7.5) and 100 mM NaCl. Each sample was evaluated in triplicate, and measurements were recorded within a 20-min time frame while temperature was maintained.

NMR—All NMR experiments were performed on a 600-MHz Varian Inova spectrometer using a cryogenic HCN probe capable of ^{19}F NMR. Spectra of β_2AR in DDM were acquired at 25 °C, whereas those in MNG-3 were acquired at 30 °C. Typical spectra were acquired with 8192 scans and a repetition time of 1 s, with a $\pi/2$ pulse length of 14.5 μs and an acquisition time of 0.25 s. Spectra were processed with MestReNova software. Free induction decay signals, consisting of 14,000 complex points in the direct dimension, were typically linear predicted for the first two to four points in the free induction decay, zero-filled to 32,000 points, and apodized with a Lorentzian filter equivalent to 30-Hz broadening (DDM) and 4-Hz broadening (MNG).

RESULTS

To assess the possibility of distinct functional states, we employed a trifluoromethyl tag ($-COCF_3$) located on Cys-265, which is near the cytosolic water interface of transmembrane domain 6. As shown in Fig. 1*A*, crystal structures of inactive and active β_2ARs demonstrate that transmembrane domain 6 is displaced outward from the helical bundle upon activation, such that Cys-265 becomes more solvent-exposed in the active state. Crystal structures of the active and inactive states suggest that this labeling site is ideal to probe conformational equilibria and possible exchange between functional states. ^{19}F NMR is ideally suited for such studies because this probe is exquisitely sensitive to solvent exposure. Thus, the extent of activation of the protein or, equivalently, the outward displacement of Cys-265 can be directly monitored by ^{19}F NMR using a single labeling site. To avoid labeling other cysteines, a fully functional mutant was prepared in which four labile cysteines were replaced with valine (C77V), serine (C275S), and alanine (C378A and C406A), as shown in Fig. 1*B*. Cys-341 was, however, not mutated, in an effort to retain the β_2AR palmitoylation site, for receptor expression and function.

β_2AR Interconverts between Inactive and Active States on an Intermediate or Fast Time Scale in DDM Micelles—Fig. 2 shows representative ^{19}F NMR spectra of β_2AR in DDM detergent micelles from the perspective of a single trifluoromethyl probe located at Cys-265. The spectra, resulting from saturating amounts of either inverse agonist (carazolol) or agonist (BI-

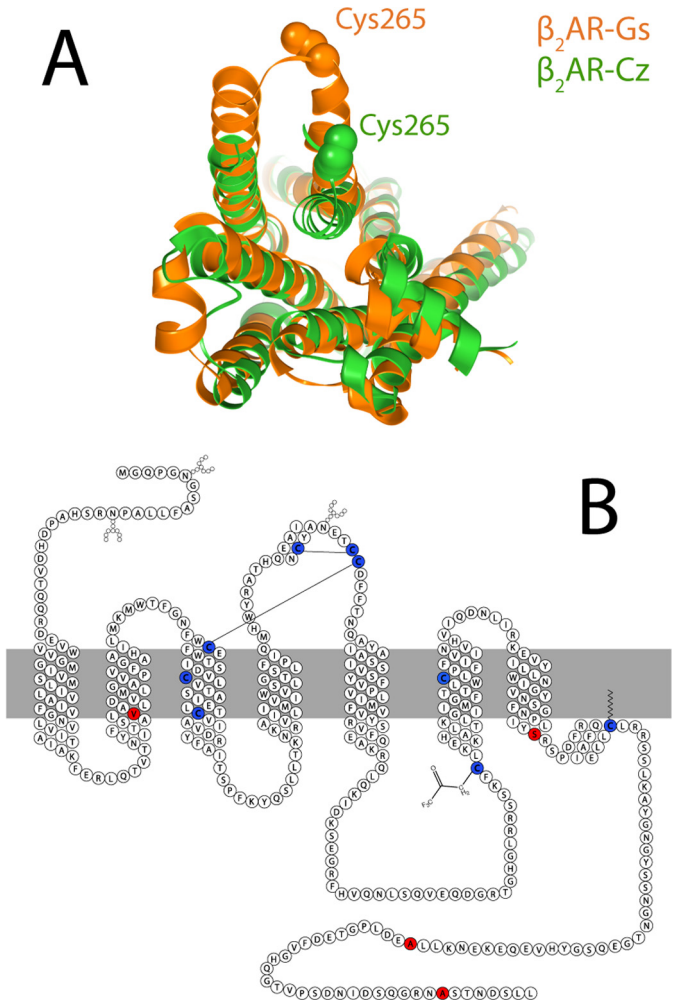

FIGURE 1. *A*, overlay of x-ray crystal structures of β_2AR stabilized by either the inverse agonist carazolol (*Cz*; shown in *green*) or the stimulatory G protein Gα_s (shown in *orange*). *B*, sequence and secondary structure of β_2AR showing cysteine residues that are retained for stability and labeling (*blue*) and those that are removed (*red*) to avoid excess labeling. *Solid lines* indicate disulfide linkages.

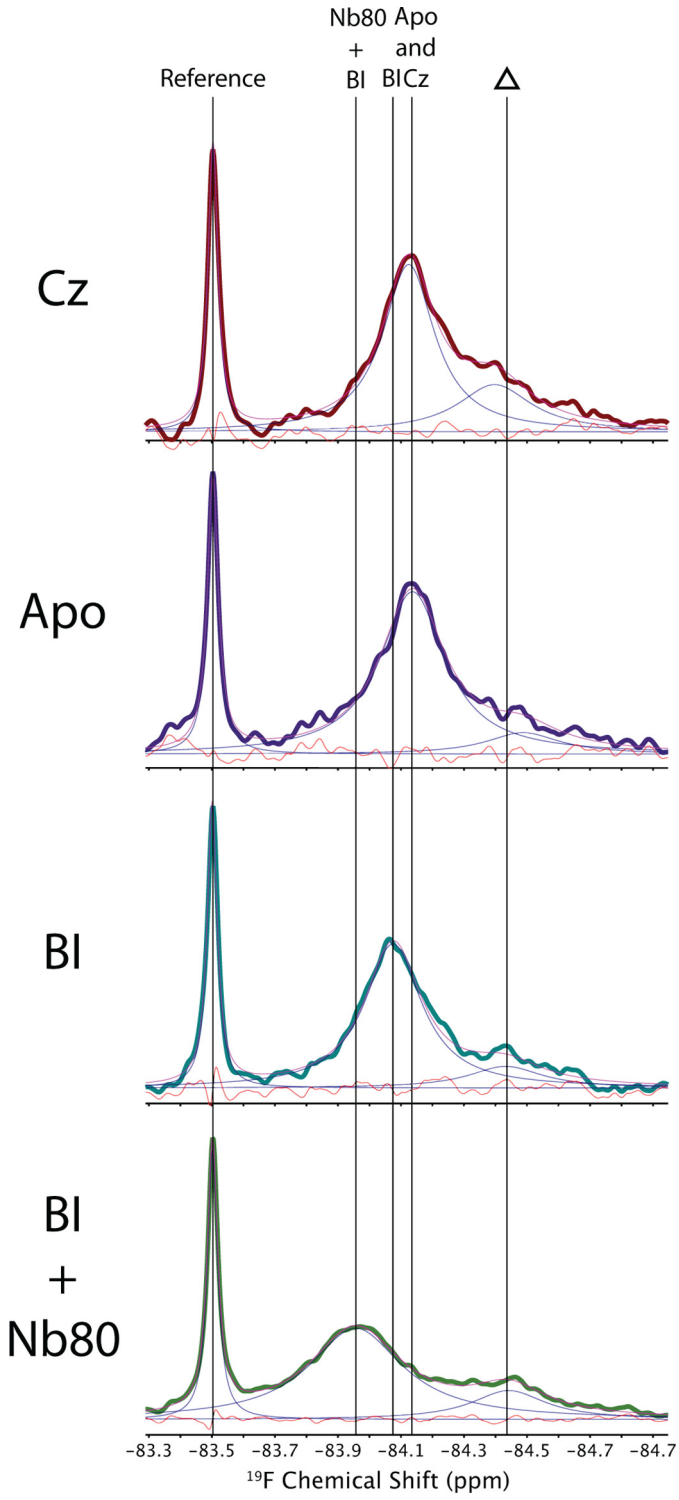

FIGURE 2. **^{19}F NMR spectra of β_2AR reconstituted in DDM micelles at 25 °C.** Note that the *leftmost peak* represents a small molecule used as a reference, whereas the barely detectable peak to the right (indicated by a *triangle*) represents a residually labeled cysteine on β_2AR, the spectral area of which remains independent of ligand. The *orange line* designates residual error resulting from deconvoluting the spectrum. *Cz*, carazolol; *BI*, BI-167107.

167107), are both well represented by a single motionally averaged state, as shown by the deconvolutions and residual errors. Note that a second weak peak, near −84.5 ppm, is also partially labeled and may arise from another labeled cysteine residue. Although the resonance associated with this second site is unchanged upon addition of ligand, the main resonance associated with Cys-265 shifts downfield upon activation with BI-167107. The addition of an antibody-derived single domain protein (Nb80), meant to mimic Gα_s (21) and shift the equilibrium toward complete activation, also gives rise to a single Lorentzian line and a further downfield shift. The spectrum associated with Cys-265 thus appears as one resonance, which is shifted downfield upon activation by BI-167107 and further downfield by BI-167107 plus Nb80. Fig. 3 reflects this trend in shift with increasing activation. Because the apo-, carazolol-, and BI-167107-saturated states of β_2AR are expected to adopt an equilibrium between active and inactive conformers, it is perhaps surprising to observe a single peak. Given the trend in chemical shift with activation, we conclude that the spectra are a result of intermediate or fast conformational exchange between two (or more) states on a time scale greater than the range of chemical shifts (*i.e.* ≥100 Hz).

Recently, Liu *et al.* (22) reported ^{19}F NMR studies of a similar variant of β_2AR in DDM micelles, as a function of a wide range

of ligands, by separately labeling Cys-265 and Cys-327$^{7.54}$ with trifluoroethane thiol (*i.e.* β_2AR^{TET}). In this study, the authors identified two resonances associated with Cys-265, separated by ~0.75 ppm (~430 Hz). By investigating the effect of a wide range of ligands on the spectra, the authors were able to conclude that these resonances represented inactive and active states. In recent model studies, we observed that $-COCF_3$ probes provide relatively narrow lines but significantly less chemical shift dispersion (by a factor of ~5) than other cysteine-specific trifluoromethyl probes such as trifluoroethane thiol. Thus, it is possible that the active and inactive states are in slow exchange in the presence of trifluoroethane thiol probes (*i.e.* exchange rates <430 Hz), whereas this would represent a fast exchange limit when $-COCF_3$ probes are used. The coincident downfield shift of a single ^{19}F NMR resonance upon progressive activation (*i.e.* inverse agonist → apo → agonist → agonist plus Nb80) is thus highly suggestive of an equilibrium shift between two or more states in fast exchange (≥100 Hz).

Subtle effects of ligand, in terms of orientational order and dynamics of Cys-265, can also be discerned from measurements of ^{19}F NMR relaxation times (T_1 and T_2). Following the so-called model-free approach, we can interpret T_1 and T_2 measurements in terms of a global micelle tumbling time (τ_M), an order parameter (S), and a local correlation time (τ_e), which define the amplitude and frequency of local motions at Cys-265 (23, 24). In our case, we assumed that ^{19}F T_1 and T_2 relaxation is dominated by chemical shift anisotropy, and we made use of T_1 and T_2 measurements at 600 MHz (^1H Larmor frequency) to obtain a more reliable estimate of S and τ_e. τ_M is assumed to result from isotropic reorientation and is estimated from experimental measures of the radius of hydration (r_H) of the β_2AR micelle. r_H is in turn measured from pulsed field gradient-stimulated echo diffusion measurements using the protein ^1H aromatic signal. Note that r_H is measured for both carazolol-stabilized β_2AR and Nb80-stabilized β_2AR. Table 1 summarizes the measured trends in T_1 and T_2, along with measurements of r_H for the ligand-associated and Nb80-associated samples. Fig. 4 reveals a trend of increased local order and decreased τ_e with activation toward the nanobody-stabilized fully active state. Although apo-β_2AR exhibits basal activity and thus transits between active and inactive states, we envisage the addition of Nb80 to fully stabilize a specific active state. Assuming the relative energy of the Nb80 state is such that the inactive states are no longer accessible, the order parameter of the active state would be expected to increase, as observed. Although the amplitudes of local motions are decreased (increased S), the local reorientational frequency ($1/\tau_e$) appears to increase, upon activation, in DDM micelles. These amplitudes and frequencies likely reflect exchange between states and possible conformational substates associated with the GPCR (25).

β_2AR Interconverts between Inactive and Active States on a Slow Time Scale in MNG-3—In an effort to improve protein stability and resolution, we explored the use of newly developed MNG-3 detergents, which consist of two maltose units in their hydrophilic domain and two *n*-decyl chains appended to a quaternary central carbon (17). MNG is known to stabilize integral membrane proteins at higher temperatures, which is clearly an advantage in NMR applications because T_2 increases dramatically with temperature. Fig. 5 shows ^{19}F NMR spectra of β_2AR stabilized in MNG-3 micelles at 30 °C as a function of ligand. Although we again observe an upfield peak, the area of which is independent of ligand, it is possible to deconvolute three Lorentzian lines and thus three distinct states associated with Cys-265 for carazolol-saturated β_2AR. Note that the residual fitting error is comparable with the noise across the spectra shown in Fig. 5, whereas residual errors are slightly higher than noise, if we assume that Cys-265 can be represented by only two peaks. The existence of three states was also confirmed by directly measuring T_2 and comparing the measured T_2 values to

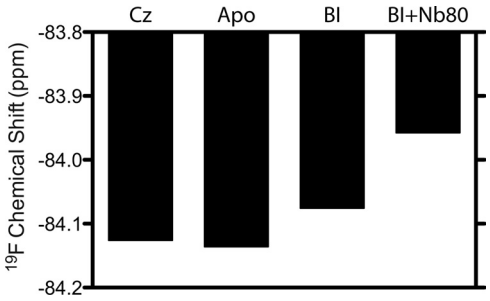

FIGURE 3. **^{19}F NMR chemical shift trends at Cys-265 as a function of activation in DDM micelles.** *Cz*, carazolol; *BI*, BI-167107.

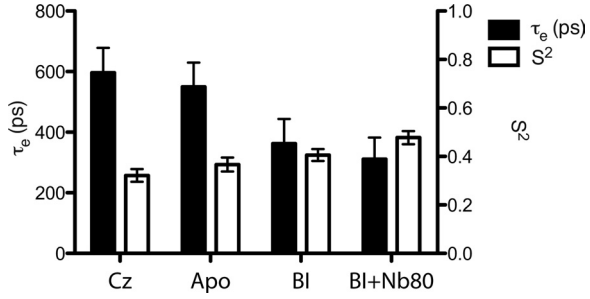

FIGURE 4. **Estimates of S and τ_e at Cys-265 as a function of activation of β_2AR (saturating concentrations of inverse agonist → apo → BI-167107 agonist → BI-167107 agonist plus Nb80).** Estimates of local orientational order and dynamics were based upon measurements of ^{19}F T_1 and T_2 at 600 MHz. *Black bars* represent τ_e, and *white bars* represent S^2. *Cz*, carazolol; *BI*, BI-167107.

TABLE 1

Measured chemical shifts, T_1 and T_2 relaxation times, and fitted internal correlation times and squared order parameters associated with the trifluoromethyl tag on Cys-265 of β_2AR in DDM micelles

Measurements were performed at a ^{19}F Larmor frequency of 564.3 MHz at 25 °C.

	Chemical shift	T_1	T_2	τ_e	S^2
	ppm	*ms*	*ms*	*ps*	
Carazolol	−84.126	468.8 ± 47.6	1.696 ± 0.100	596.2 ± 82.4	0.3216 ± 0.0262
Apo	−84.136	475.4 ± 49.0	1.488 ± 0.086	549.4 ± 80.1	0.3665 ± 0.0287
BI-167107	−84.076	425.5 ± 29.8	1.349 ± 0.046	362.2 ± 81.2	0.4057 ± 0.0246
BI-167107 + Nb80	−83.958	463.1 ± 37.2	0.952 ± 0.054	310.7 ± 71.5	0.4778 ± 0.0270

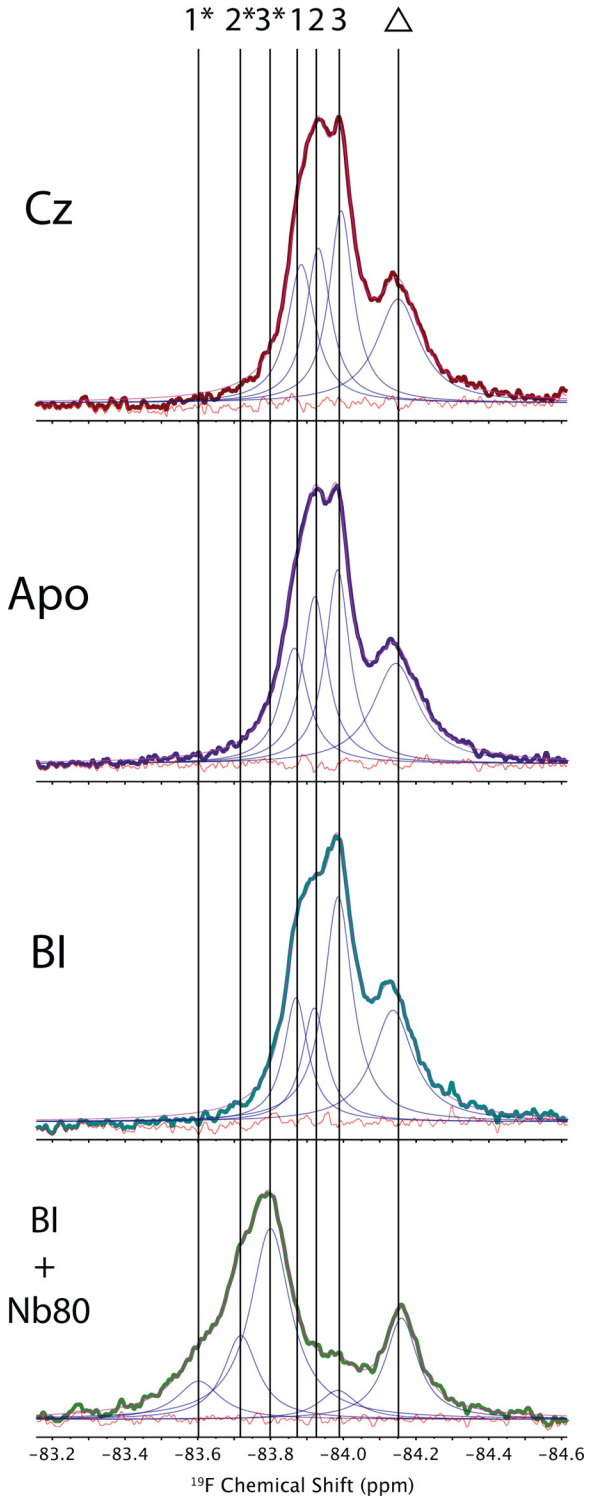

FIGURE 5. **^{19}F NMR spectra of β_2AR reconstituted in MNG micelles at 30 °C.** Note that the peak to the right (indicated by a *triangle*) represents a residually labeled cysteine on β_2AR, the spectral area of which remains independent of ligand. The presence of a second partially labeled site was corroborated by subsequent ^{19}F NMR spectra from proteinase K digests. *Cz*, carazolol; *BI*, BI-167107.

those extracted from the spectral convolution (*i.e.* $T_2 = 1/(\pi \times \Delta\nu)$, where $\Delta\nu$ represents the deconvoluted line width). Moreover, the progressive activation of β_2AR, as monitored by spectra of the apo state and the BI-167107-saturated state, reveals

TABLE 2
Estimates of the CMC, ΔH, and ΔS associated with micellization of DDM and MNG-3 based on isothermal titration calorimetry measurements.
In this analysis, we assume that ΔH associated with micellization of MNG-3 is the same as that measured for DDM.

Detergent	CMC	ΔG	ΔH	ΔST
	μM	kJ/mol	kJ/mol	kJ/mol
DDM	130	−32.7	−2.27	30.4
MNG-3	0.0113	−56.2	−2.27	53.9

the presence of these same three peaks, differing only in their intensities. We interpret this to mean that Cys-265 samples three distinct states (labeled *1*, *2*, and *3* in Fig. 5), the populations of which depend sensitively on ligand. Finally, the addition of Nb80 to the BI-167107-saturated sample resulted, upon deconvolution, in a prominent peak (labeled *3** in Fig. 5), in addition to two minor peaks (labeled *1** and *2**). Although the crystal structure of the β_2AR-Nb80 complex suggests that the Cys-265 side chain terminus is >5 Å from the van der Waals surface of the nanobody (21), it is possible that electrostatic effects from the bound nanobody may still influence the observed shifts. Thus, 3* likely represents the fully active state of β_2AR, which is shifted largely because of a change in electrostatic environment upon binding by Nb80. Similarly, 1* and 2* may correspond to residual inactive or partially active states 1 and 2, the shifts of which again appear more downfield due to the long-range electrostatic effects of Nb80 on the CF_3 probe. Thus, the use of MNG-3 detergents results in at least three Lorentzian lines with chemical shifts that are independent of the extent of activation (*i.e.* carazolol → apo → BI-167107). Rather, the proportion of each peak depends on ligand and points toward a complex equilibrium, which is in the slow exchange limit (*i.e.* exchange rates <70 Hz), in stark contrast to our observations of β_2AR in DDM micelles.

DISCUSSION

The above experiments on β_2AR with DDM and MNG-3 reveal that the detergent host can substantially alter the exchange rate between functional conformers from the fast or intermediate motional regime to a slow motional regime. The majority of detergents used in NMR studies of membrane proteins exhibit millimolar CMCs. Table 2 compares experimentally determined CMCs and associated enthalpic and entropic contributions to micellization for DDM and MNG-3. We found that the CMC of DDM is 130 μM, whereas that of MNG-3 is 4 orders of magnitude lower (11.3 nM). The CMC of DDM was determined by both isothermal titration calorimetry, as shown in Fig. 6, and fluorescence via the hydrophobic fluorophore 1-anilino-8-naphthalene sulfonate, which selectively partitions into micelles. As the CMC of MNG-3 is significantly lower, both fluorescence and isothermal titration calorimetry could not be used; rather, surface tension measurements, via a force tensiometer, were employed to measure the CMC of MNG-3 (26).

Using the CMC, we can estimate the detergent off-rate, assuming that the on-rate is diffusion-limited. In the case of DDM, the detergent diffusion coefficient, which greatly exceeds that of the micelle, was measured and found to be 3.8 ×

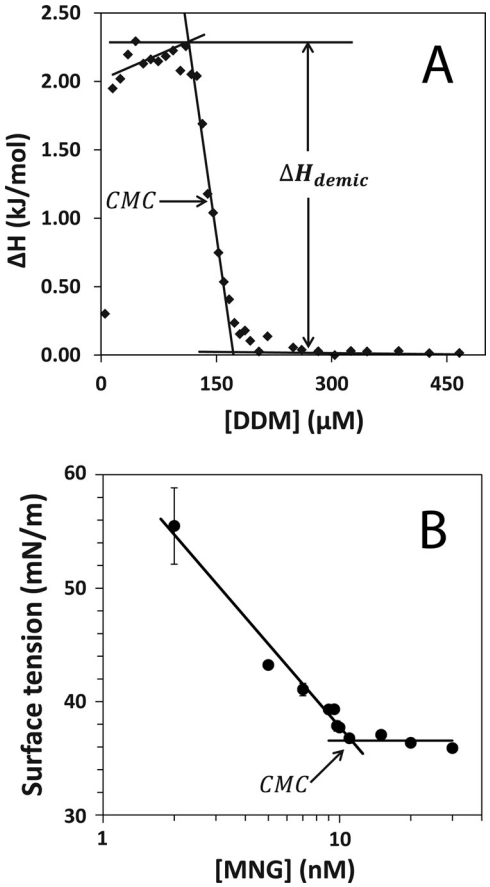

FIGURE 6. *A*, isothermal titration calorimetry enthalpogram of DDM, where ΔH_{demic} is −2.27 kJ/mol, and the CMC, determined from a first derivative plot of the enthalpogram, is estimated to be 0.13 mM. *B*, surface tension-based measurement of MNG-3 showing the CMC to be 11.3 nM.

10^{-10} m^2/s at 25 °C. In this case, the detergent on-rate is approximated by Equation 1,

$$k_{on} \approx 4\pi R^* D_{monomer} N_A 10^3 \quad \text{(Eq. 1)}$$

where R^* represents the radius associated with the collisional area (*i.e.* radius of micelle plus radius of detergent), N_A represents Avogadro's number, and $D_{monomer}$ represents the monomer diffusion constant. R^* was estimated to be 3.7 nm based on an aggregate number of 110 (27). We then obtain an on-rate of 1.1×10^{10} M^{-1} s^{-1}. The rate constants k_{on} and k_{off} may be related to the concentration of micelles, monomers, and micelles missing one detergent via stepwise micelle association expression (28) (Equation 2).

$$k_{on}[\text{monomer}][\text{micelle} - 1] = k_{off}[\text{micelle}] \quad \text{(Eq. 2)}$$

Assuming [micelle − 1] and [micelle] are equal, k_{off} is then determined by the CMC (*i.e.* [monomer]), yielding a detergent off-rate of 1.43×10^6 s^{-1}. As the CMC of MNG-3 is 10,000-fold lower than that of DDM, we therefore expect the detergent off-rate to be >4 orders of magnitude lower, under the assumption that the diffusion rates of the monomeric detergent species are similar. This amounts to an off-rate that is slow on the NMR time scale on a per detergent basis. Detergents are generally known to exchange very rapidly with the solvent (29). For example, the CMC of dodecylphosphocholine is even higher than that of DDM (*i.e.* faster off-rate). Thus, MNG-3, the CMC of which is in fact comparable with that of a phospholipid, represents an exception to the norm. The relative stability afforded by very slow exchanging MNG-3 has been observed previously in functional assays in which the loss of ligand ([^{3}H]dihydroalprenolol) was monitored with time upon dilution (30). On the basis of the differences in the spectra of DDM-stabilized β_2AR and MNG-3-stabilized β_2AR, we propose that detergent exchange directly influences the activation energies between functional states in the GPCR. The gross changes in structure between inactive and active states, as illustrated in Fig. 1, likely involve a change in hydrophobic surface area and a rearrangement in detergent coatings. In cases in which detergent off-rates are sufficiently slow, detergent exchange may thus represent the rate-limiting step in interconversion between functional states. Moreover, the activation energies between functional states in physiological membranes are likely closer to those obtained in the presence of low CMC detergents (17).

Polytopic α-helical membrane proteins are well known to exhibit exchange broadening through intermediate time scale motions to the extent that, in many studies of GPCRs, which could be expressed from *Escherichia coli* in inclusion bodies and reconstituted in detergent micelles, only the mobile loop residues were observed (14). GPCRs are also inherently dynamic and complex, as evidenced by the ligand-selective G_s, G_i, and arrestin pathways through which β_2AR signals. Nevertheless, progress by others (13) with a seven-transmembrane GPCR analog and preliminary experiments on a 320-residue β_1AR, thermostabilized through limited mutagenesis, suggest that it may be possible to limit intermediate time scale conformational exchange for the sake of resolution and backbone assignment. The use of novel detergents such as MNG-3 in this study of β_2AR provided a spectroscopic glimpse of three distinct states, which were effectively invisible in DDM. Thus, detergents also profoundly affect stability and exchange rates between states.

CONCLUSION

On the basis of the kinetic and thermodynamic comparisons of the above detergents and the prominent differences in exchange rates between functional states of β_2AR, we propose that detergent exchange strongly couples with GPCR functional dynamics. MNG-3 off-rates are sufficiently slow that distinct functional states are now observed, and overall resolution is improved. Moreover, exchange rates between functionally distinct conformers in lipid bilayers are likely closer to those observed in very low CMC assemblies such as MNG-3 rather than conventional detergent micelles (32). Protein stability is also increased with such low CMC detergents (17). The above ^{19}F NMR experiments may be performed 5–7 °C higher in MNG-3 than in DDM over periods of days to weeks. It should be noted that there are other amphiphilic hosts such as amphipols (33–35) and nanodiscs (36, 37) in which a similar if not better protein-stabilizing environment is attained, where exchange between functional states is possibly equally representative of physiological conditions. However, for the moment, new detergents such as MNG are a necessary evil for NMR purposes because the aggregate mass is minimal, and thus, T_2 is optimal for

purposes of resolution and INEPT (insensitive nuclei enhanced by polarization transfer) transfers (31).

Acknowledgments—We thank Alexandar Hansen (University of Toronto) for assistance in simulating order parameters and correlation times from ^{19}F NMR relaxation experiments. We also thank Prof. Edgar Acosta and Sheng Xu (University of Toronto) for performing the CMC measurements of MNG-3 and Dr. Ron Dror (D. E. Shaw Research) for guidance and helpful comments.

REFERENCES

1. Tate, C. G., and Schertler, G. F. (2009) Engineering G protein-coupled receptors to facilitate their structure determination. *Curr. Opin. Struct. Biol.* **19,** 386–395
2. Kobilka, B. K. (2011) Structural insights into adrenergic receptor function and pharmacology. *Trends Pharmacol. Sci.* **32,** 213–218
3. Kobilka, B., and Schertler, G. F. (2008) New G protein-coupled receptor crystal structures: insights and limitations. *Trends Pharmacol. Sci.* **29,** 79–83
4. Chill, J. H., Louis, J. M., Miller, C., and Bax, A. (2006) NMR study of the tetrameric KcsA potassium channel in detergent micelles. *Protein Sci.* **15,** 684–698
5. Baker, K. A., Tzitzilonis, C., Kwiatkowski, W., Choe, S., and Riek, R. (2007) Conformational dynamics of the KcsA potassium channel governs gating properties. *Nat. Struct. Mol. Biol.* **14,** 1089–1095
6. Schnell, J. R., and Chou, J. J. (2008) Structure and mechanism of the M2 proton channel of influenza A virus. *Nature* **451,** 591–595
7. Traaseth, N. J., Shi, L., Verardi, R., Mullen, D. G., Barany, G., and Veglia, G. (2009) Structure and topology of monomeric phospholamban in lipid membranes determined by a hybrid solution and solid-state NMR approach. *Proc. Natl. Acad. Sci. U.S.A.* **106,** 10165–10170
8. Zhou, Y., Cierpicki, T., Jimenez, R. H., Lukasik, S. M., Ellena, J. F., Cafiso, D. S., Kadokura, H., Beckwith, J., and Bushweller, J. H. (2008) NMR solution structure of the integral membrane enzyme DsbB: functional insights into DsbB-catalyzed disulfide bond formation. *Mol. Cell* **31,** 896–908
9. Van Horn, W. D., Kim, H. J., Ellis, C. D., Hadziselimovic, A., Sulistijo, E. S., Karra, M. D., Tian, C., Sönnichsen, F. D., and Sanders, C. R. (2009) Solution nuclear magnetic resonance structure of membrane integral diacylglycerol kinase. *Science* **324,** 1726–1729
10. Hiller, S., Garces, R. G., Malia, T. J., Orekhov, V. Y., Colombini, M., and Wagner, G. (2008) Solution structure of the integral human membrane protein VDAC-1 in detergent micelles. *Science* **321,** 1206–1210
11. Gautier, A., Mott, H. R., Bostock, M. J., Kirkpatrick, J. P., and Nietlispach, D. (2010) Structure determination of the seven-helix transmembrane receptor sensory rhodopsin II by solution NMR spectroscopy. *Nat. Struct. Mol. Biol.* **17,** 768–774
12. Liang, B., and Tamm, L. K. (2007) Structure of outer membrane protein G by solution NMR spectroscopy. *Proc. Natl. Acad. Sci. U.S.A.* **104,** 16140–16145
13. Nietlispach, D., and Gautier, A. (2011) Solution NMR studies of polytopic α-helical membrane proteins. *Curr. Opin. Struct. Biol.* **21,** 497–508
14. Kim, H. J., Howell, S. C., Van Horn, W. D., Jeon, Y. H., and Sanders, C. R. (2009) Recent advances in the application of solution NMR spectroscopy to multi-span integral membrane proteins. *Prog. Nucl. Magn. Reson. Spectrosc.* **55,** 335–360
15. Tamm, L., and Liang, B. (2006) NMR of membrane proteins in solution. *Prog. Nucl. Magn. Reson. Spectrosc.* **48,** 201–210
16. Kang, C., and Li, Q. (2011) Solution NMR study of integral membrane proteins. *Curr. Opin. Chem. Biol.* **15,** 560–569
17. Chae, P. S., Rasmussen, S. G., Rana, R. R., Gotfryd, K., Chandra, R., Goren, M. A., Kruse, A. C., Nurva, S., Loland, C. J., Pierre, Y., Drew, D., Popot, J. L., Picot, D., Fox, B. G., Guan, L., Gether, U., Byrne, B., Kobilka, B., and Gellman, S. H. (2010) Maltose-neopentyl glycol (MNG) amphiphiles for solubilization, stabilization, and crystallization of membrane proteins. *Nat. Methods* **7,** 1003–1008
18. Yao, X. J., Vélez Ruiz, G., Whorton, M. R., Rasmussen, S. G., DeVree, B. T., Deupi, X., Sunahara, R. K., and Kobilka, B. (2009) The effect of ligand efficacy on the formation and stability of a GPCR-G protein complex. *Proc. Natl. Acad. Sci. U.S.A.* **106,** 9501–9506
19. Bokoch, M. P., Zou, Y., Rasmussen, S. G., Liu, C. W., Nygaard, R., Rosenbaum, D. M., Fung, J. J., Choi, H. J., Thian, F. S., Kobilka, T. S., Puglisi, J. D., Weis, W. I., Pardo, L., Prosser, R. S., Mueller, L., and Kobilka, B. K. (2010) Ligand-specific regulation of the extracellular surface of a G protein-coupled receptor. *Nature* **463,** 108–112
20. Tsamaloukas, A. D., Beck, A., and Heerklotz, H. (2009) Modeling the micellization behavior of mixed and pure *n*-alkyl maltosides. *Langmuir* **25,** 4393–4401
21. Rasmussen, S. G., Choi, H. J., Fung, J. J., Pardon, E., Casarosa, P., Chae, P. S., DeVree, B. T., Rosenbaum, D. M., Thian, F. S., Kobilka, T. S., Schnapp, A., Konetzki, I., Sunahara, R. K., Gellman, S. H., Pautsch, A., Steyaert, J., Weis, W. I., and Kobilka, B. K. (2011) Structure of a nanobody-stabilized active state of the β_2-adrenoceptor. *Nature* **469,** 175–180
22. Liu, J. J., Horst, R., Katritch, V., Stevens, R. C., and Wüthrich, K. (2012) Biased signaling pathways in β_2-adrenergic receptor characterized by ^{19}F NMR. *Science* **335,** 1106–1110
23. Lipari, G., and Szabo, A. (1982) Model-free approach to the interpretation of nuclear magnetic resonance relaxation in macromolecules. 2. Analysis of experimental results. *J. Am. Chem. Soc.* **104,** 4559–4570
24. Lipari, G., and Szabo, A. (1982) Model-free approach to the interpretation of nuclear magnetic resonance relaxation in macromolecules. 1. Theory and range of validity. *J. Am. Chem. Soc.* **104,** 4546–4559
25. Deupi, X., and Kobilka, B. K. (2010) Energy landscapes as a tool to integrate GPCR structure, dynamics, and function. *Physiology* **25,** 293–303
26. Acosta, E. J., Harwell, J. H., and Sabatini, D. A. (2004) Self-assembly in linker-modified microemulsions. *J. Colloid Interface Sci.* **274,** 652–664
27. Møller, J. V., and le Maire, M. (1993) Detergent binding as a measure of hydrophobic surface area of integral membrane proteins. *J. Biol. Chem.* **268,** 18659–18672
28. Aniansson, E. A., and Wall, S. N. (1974) Kinetics of stepwise micelle association. *J. Phys. Chem.* **78,** 1024–1030
29. Thomas, M. J., Pang, K., Chen, Q., Lyles, D., Hantgan, R., and Waite, M. (1999) Lipid exchange between mixed micelles of phospholipid and Triton X-100. *Biochim. Biophys. Acta* **1417,** 144–156
30. Rasmussen, S. G., DeVree, B. T., Zou, Y., Kruse, A. C., Chung, K. Y., Kobilka, T. S., Thian, F. S., Chae, P. S., Pardon, E., Calinski, D., Mathiesen, J. M., Shah, S. T., Lyons, J. A., Caffrey, M., Gellman, S. H., Steyaert, J., Skiniotis, G., Weis, W. I., Sunahara, R. K., and Kobilka, B. K. (2011) Crystal structure of the β_2-adrenergic receptor-G_s protein complex. *Nature* **477,** 549–555
31. Cavanagh, J., Fairbrother, W. J., Palmer, A. G., and Skelton, N. J. (2007) *Protein NMR Spectroscopy: Principles and Practice*, 2nd Ed., Academic Press, New York
32. Kusnetzow, A. K., Altenbach, C., and Hubbell, W. L. (2006) Conformational states and dynamics of rhodopsin in micelles and bilayers. *Biochemistry* **45,** 5538–5550
33. Popot, J. L. (2010) Amphipols, nanodiscs, and fluorinated surfactants: three nonconventional approaches to studying membrane proteins in aqueous solutions. *Annu. Rev. Biochem.* **79,** 737–775
34. Popot, J. L., Althoff, T., Bagnard, D., Banères, J. L., Bazzacco, P., Billon-Denis, E., Catoire, L. J., Champeil, P., Charvolin, D., Cocco, M. J., Crémel, G., Dahmane, T., de la Maza, L. M., Ebel, C., Gabel, F., Giusti, F., Gohon, Y., Goormaghtigh, E., Guittet, E., Kleinschmidt, J. H., Kühlbrandt, W., Le Bon, C., Martinez, K. L., Picard, M., Pucci, B., Sachs, J. N., Tribet, C., van Heijenoort, C., Wien, F., Zito, F., and Zoonens, M. (2011) Amphipols from A to Z. *Annu. Rev. Biophys.* **40,** 379–408
35. Catoire, L. J., Damian, M., Giusti, F., Martin, A., van Heijenoort, C., Popot, J. L., Guittet, E., and Banères, J. L. (2010) Structure of a GPCR ligand in its receptor-bound state: leukotriene B4 adopts a highly constrained conformation when associated to human BLT2. *J. Am. Chem. Soc.* **132,** 9049–9057
36. Bayburt, T. H., and Sligar, S. G. (2010) Membrane protein assembly into nanodiscs. *FEBS Lett.* **584,** 1721–1727
37. Serebryany, E., Zhu, G. A., and Yan, E. C. Y. (2012) Artificial membrane-like environments for *in vitro* studies of purified G protein-coupled receptors. *Biochim. Biophys. Acta* **1818,** 225–233